超音波による内膜中膜複合体厚計測のためのテンプレートマッチングによる頸動脈後壁の境界自動検出に関する研究

	ナビラ　ビンティ　イブラヒム
氏　　名	Nabilah Binti Ibrahim
授　与　学　位	博士（工学）
学位授与年月日	平成２５年３月２７日
学位授与の根拠法規	学位規則第４条第３項
研究科，専攻の名称	東北大学大学院工学研究科（博士課程）電子工学専攻
学位論文題目	超音波による内膜中膜複合体厚計測のためのテンプレート マッチングによる頸動脈後壁の境界自動検出に関する研究
指　導　教　員	東北大学教授　金井　浩
論文審査委員	主査　東北大学教授　金井　浩　　東北大学教授　川又 政征 東北大学教授　吉澤　誠　　東北大学准教授　長谷川英之

1. Introduction

Cardiovascular diseases (CVDs) are responsible for over 17.3 million deaths yearly and are the leading causes of the death in the world.[1] Since the atherosclerosis is considered to be the main cause of the CVDs, it is important to diagnose the early-stage atherosclerosis. Intima-media thickness (IMT) correlates very well with pathohistologic measurements which evaluated by microscopic examination, for assessing cardiovascular risk,[2] where the IMT is commonly defined by the distance between the lumen-intima boundary (LIB) and the media-adventitia boundary (MAB) of the posterior carotid artery wall. Thus, the IMT measurement is essential for diagnosis of early-stage atherosclerosis. Number of methods are capable to detect the LIB and MAB of the posterior carotid arterial wall. The intensity gradient[3] method is frequently misdetects the MAB owing to the effect of echoes from intima-media complex (IMC). Golemati *et al.* used another approach by using the segmentation of specific shape in an ultrasonic image so that the lines of the LIB and MAB could be detected.[4] However, the method can be applied to only the straight carotid arterial wall. For the measurement of the IMT using a dynamic programming method, Liang *et al.* were able to detect the boundaries precisely.[5] However, their method requires retraining when the image characteristics change which is time consuming. To overcome and/or reduce the drawback of these methods, previous efforts have been done to automatically assess the LIB and MAB positions using template matching between the echo models (LIB and MAB echo models) and measured *in vivo* RF echo (using RF signal[6,7] and envelope[8]). The positions of the models, which give the minimum difference between the measured and model signals, are determined as the boundaries. However, the difference between the echo model and the measured *in vivo* RF echo and even that between the echo model and the reference RF signal are significant. Furthermore, the results obtained are insufficient since the center frequencies of the echo models that need to be fitted with the measured *in vivo* RF echoes are fixed. A model with a fixed center frequency is not suitable because the center frequency of the echo signal from an arterial wall differs from person to person due to frequency dependent attenuation. In the present study, the echo model is improved from the previous one[6-8] by creating the echo model from the transmitted wave measured with a hydrophone. Moreover, the center frequency and the phase of the echo model are changed gradually to find the best fit between the echo models and the measured *in vivo* RF echoes. As a result, the proposed method shows the better result than the previous one which lead to the accurate boundary detection.

2. Principle

2.1 Measurement of Received Echo Model

In this study, an echo model $\hat{z}(f_0,T_{d1},T_{d2},a_1,a_2,nT_s)$ is matched with the measured *in vivo* RF echo $x(nT_s)$ from the posterior carotid arterial wall by evaluating the difference $\alpha(f_0,T_{d1},T_{d2},a_1,a_2;\tau_1,\tau_2)$ between them using the mean squared error (MSE) method. The echo model is sum of two received echo models $\hat{z}_i(f_0,T_d,a;nT_s)$, which correspond to a received wave $y'(f_0,T_d',a;nT_s')$ calculated from a transmitted wave measured with a hydrophone. The transmitted wave $g_T(t)$ was emitted in a water tank with a linear-array transducer at 10 MHz (UST-5410, ALOKA), which is connected to a modified ultrasonic diagnosis equipment (SSD-6500, ALOKA), and was measured with a hydrophone (MHA9-150, FORCE) placed at the distance d of 13.7 mm, associated with the focal distance. The wave was averaged for 64 times, recorded by a digital oscilloscope (TDS 2014, Tektronix) at a sampling frequency of 1 GHz at 8-bit resolution. Figure 1 shows the block diagram of the process that motivates to obtain a received wave from a transmitted wave. The transmitted wave is assumed as the one-way propagation wave with the delay τ and the reflected wave as the round-trip propagation wave with the propagation time of 2τ. The process starts with the electrical signal $x(t)$ that excites the piezo elements. The signal is apparently very short in time as could be assumed to be an impulse. The piezo elements transform it to the transmitted wave $g_T(t)$. At this stage, the transmitted wave is measured with the hydrophone. Note that the wave encounters the scatterer and turn back to the transducer as the reflected wave $Ag_T(t)$ with reflection factor $S(f)=A$ (A: real constant) when a scatterer is placed along the way of the propagation of the transmitted wave. In this process, the reflection factor $S(f)$ is assumed not to change with frequency. The reflected wave $Ag_T(t)$ that turn back to the same transducer is transformed again by piezo elements, whose response is $g_R(t)$, to the received wave $y(t)=Ag_T(t)*g_R(t)$, where * denotes convolution. Since the transmitting and receiving elements are same, $g_T(t)=g_R(t)$ is appropriate. Thus, the

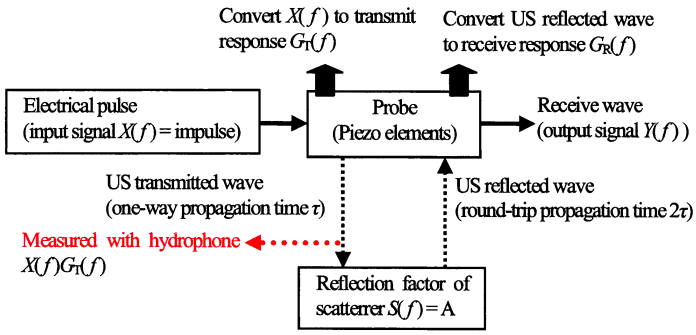

Figure 1 Frequency-domain block diagram of the process that occurs when the transmitted wave encounters scatterer.

received wave (output) $y(t)$ of the overall process can be written as

$$Y'(f)=\left\{G_T(f)e^{j2\pi f\tau}X(f)G_R(f)S(f)\right\}\cong \mathrm{A}\{G(f)\}^2. \quad (1)$$

where $Y(f), G_R(f), G_T(f)$, and $X(f)$ are frequency spectra of $y(f), g_R(f), g_T(f)$, and $x(t)$, respectively. In this work, the time delay due to round-trip propagation of the received wave is modified to be same with the time delay due to one-way propagation of the transmitted wave of τ so that the difference between the transmitted wave and the received wave could be observed at the same time. Therefore, the received wave $y'(t)$, is obtained as

$$Y(f)=\left\{G_T(f)X(f)G_R(f)S(f)\right\}\cong \mathrm{A}\{G(f)\}^2, \quad (2)$$

In order to account for the received ultrasonic pulse $y'(t)$ in the time domain, the inverse Fourier transform $\Im^{-1}[\bullet]$ is applied to the output $Y'(f)$, which is expressed as

$$y'(t)=\Im^{-1}[Y'(f)]=\Im^{-1}\left[\{AG(f)\}^2\right], \quad (3)$$

where $g(t)=\Im^{-1}[G(f)]$ is measured with a hydrophone.

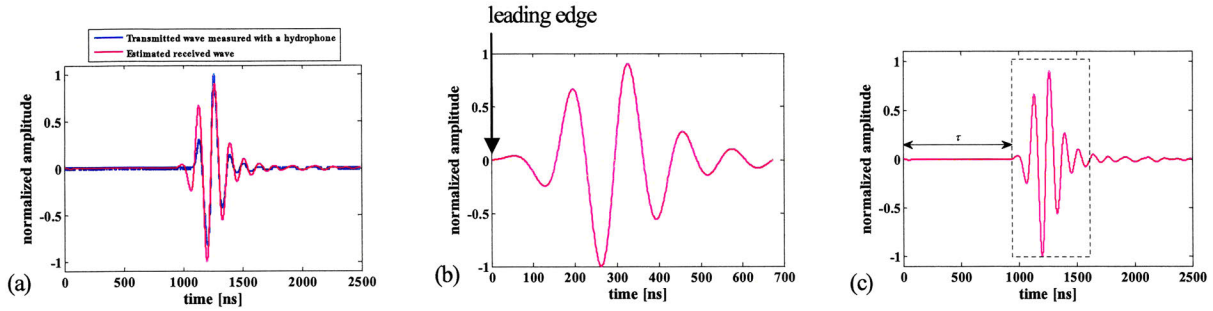

Figure 2 (a) Transmitted wave $g_T(t)$ and estimated received wave $y'(t)$. (b) Received echo model $\hat{z}(f_0,T_d,a;nT_s)$ obtained from (c) the received wave $y'(f_0,T_d',a;nT_s')$.

As shown in Fig. 2(a), the blue line is the transmitted wave $g_T(t)$ measured with a hydrophone and the pink line is the estimated received wave $y'(t)$. For the purpose of boundary detection of the carotid arterial wall, the leading edge of the $\hat{z}_i(f_0,T_d,a;nT_s)$ (i = 1: LIB, 2: MAB) has to be determined, thus, as shown in Figs. 2(b) and 2(c), the leading edge of $\hat{z}(f_0,T_d,a;nT_s)$ is determined at zero phase of $y'(f_0,T_d',a;nT_s')$ with the prior length of τ. In addition, the variables T_d and T_d' are defined as $T_d=mT_s'$ and $T_d'=\tau+T_d$. The received echo model $\hat{z}(f_0,T_d,a;nT_s)$, which is the received wave $y'(f_0,T_d',a;nT_s')$ calculated from the transmitted wave $g_T(t)$ measured with a hydrophone, is sampled at f_s' = 1 GHz ($T_s'=1/f_s'$ = 1 ns). Meanwhile, the measured *in vivo* RF echo is sampled at f_s = 40 MHz (sample spacing: 25 ns). The center frequency f_c of the received echo model is 7.4 MHz determined at the peak frequency of power spectrum of the received echo model.

2.2 Implementation of the Optimum Echo Model

To find the best fit between the echo model $\hat{z}(f_0,T_{d1},T_{d2},a_1,a_2;nT_s)$ and the measured *in vivo* RF echo $x(nT_s)$, the optimum echo model is implemented by changing the center frequency f_0 and T_{d1},T_{d2} corresponding the initial phases of the echo model gradually. To obtain the same sampling interval ($1/f_s$ = 25 ns) of those echo signals, even though the frequency f_0 of the received echo model $\hat{z}(f_0,T_d,a;nT_s)$ is changed, the sampling rate T_s of the downsampled received echo model is set to be same to the sampling rate of the measured *in vivo* RF echo $x(nT_s)$ of 40 MHz. By performing this procedure, the center frequency f_0 of the received echo model is changed gradually from 6 MHz to 8 MHz at the interval of 0.3 MHz, which corresponds to one sampling interval T_s = 1 ns to a cycle of f_c = 7.4 MHz ($T_s/T_s'*f_c$). The downsampling factor D is defined as $D=f_0/f_c*T_s'/T_s$. For the purpose to change T_{d1},T_{d2} of the echo model, the beginning point T_d (corresponding to initial phase) of the echo model is changed by a pitch of 1 ns. The combinations of all the center frequencies $\{f_0\}$ and the initial phases $\{T_d\}$ of the received echo model $\hat{z}(f_0,T_d,a;nT_s)$ could be considered to implement the optimum received echo model, thus be able to obtain the best fit with the measured *in vivo* RF echo.

2.3 Procedure of Fitting Echo Model to Measured *In Vivo* RF Echo

The proposed automated template matching method for the detection of the carotid arterial wall boundaries is realized by calculating the MSE $\alpha(f_0,T_{d1},T_{d2},a_1,a_2;\tau_1,\tau_2)$ between the measured *in vivo* RF echo $x(nT_s)$ and the echo model $\hat{z}(f_0,T_{d1},T_{d2},a_1,a_2;nT_s)$ expressed as

$$\begin{aligned}\alpha(f_0,T_{d1},T_{d2},a_1,a_2;\tau_1,\tau_2)&=\frac{1}{N}\sum_{n=0}^{N-1}\left|x(nT_s)-\hat{z}(f_0,T_{d1},T_{d2},a_1,a_2;nT_s,\tau_1,\tau_2)\right|^2+\beta,\\&=\frac{1}{N}\sum_{n=0}^{N-1}\left|x(nT_s)-\{\hat{z}_1(f_0,T_{d1},a_1;nT_s-\tau_1)+\hat{z}_2(f_0,T_{d2},a_2;nT_s-\tau_2)\}\right|^2+\beta,\\&=\frac{1}{N}\left\{\sum_{nT_s=T_1}^{T_2}\left|x(nT_s)-\hat{z}_1(f_0,T_{d1},a_1;nT_s-\tau_1)\right|^2+\sum_{nT_s=T_3}^{T_4}\left|x(nT_s)-\hat{z}_2(f_0,T_{d2},a_2;nT_s-\tau_2)\right|^2\right.\\&\quad\left.+\sum_{nT_s=T_2}^{T_3}\left|x(nT_s)-\{\hat{z}_1(f_0,T_{d1},a_1;nT_s-\tau_1)+\hat{z}_2(f_0,T_{d2},a_2;nT_s-\tau_2)\}\right|^2\right\}+\beta,\end{aligned} \quad (4)$$

where $\{T_m\}$ $(m=1, 2, 3, 4)$ is the periods illustrated in Fig. 3(a) and the variance β estimated in the L_1 and L_3 regions is defined as

$$\beta(\tau_1,\tau_2) = \underset{nT_s \in L_1, L_3}{\text{var}}\left[x(nT_s)\right], \qquad (5)$$

where $L_1 = \tau_1 - T_0$ and $L_3 = \tau_2 - \tau_1 - L_2$. Figure 3(a) shows an example of echo models when $\hat{z}_1(f_0, T_{d1}, a_1; nT_s)$ and $\hat{z}_2(f_0, T_{d2}, a_2; nT_s)$ do not overlap, which is described by the first and second subterms on the right hand-side of eq. (4). Figure 3(b) shows an example when $\hat{z}_1(f_0, T_{d1}, a_1; nT_s)$ and $\hat{z}_2(f_0, T_{d2}, a_2; nT_s)$ overlap. The overlapped echoes from the LIB and MAB is automatically taken into consideration because the MSE $\alpha(f_0, T_{d1}, T_{d2}, a_1, a_2; \tau_1, \tau_2)$ between the measured *in vivo* RF echoes $x(nT_s)$ and the echo model $\hat{z}(f_0, T_{d1}, T_{d2}, a_1, a_2; nT_s)$ is obtained using the sum of $\hat{z}_1(f_0, T_{d1}, a_1; nT_s)$ and $\hat{z}_2(f_0, T_{d2}, a_2; nT_s)$. The evaluation of the difference between the measured *in vivo* RF echo $x(nT_s)$ and the sum of the echo models $\hat{z}_1(f_0, T_{d1}, a_1; nT_s)$ and $\hat{z}_2(f_0, T_{d2}, a_2; nT_s)$ is shown by the third subterm in eq. (4). For the robust detection of LIB and MAB, the variance $\beta(nT_s \in L_1)$ is calculated as shown by the second term on the right hand-side of eq. (4), defined in eq. (5). For the calculation of variance $\beta(nT_s \in L_1)$ in the region above the LIB echo (from T_0 to T_1), since the magnitude of the echoes from the lumen is small, $\beta(nT_s \in L_1)$ is nearly zero. On the other hand, $\beta(nT_s \in L_1)$ increases when LIB echo model $\hat{z}_1(f_0, T_{d1}, a_1; nT_s)$ is fitted to the MAB echo. Note that the T_0 is the starting point of the fitting process that is manually set. The variance $\beta(nT_s \in L_3)$ of the measured signals from T_2 to T_3 is added (eq. (4)) when the echo models, $\hat{z}_1(f_0, T_{d1}, a_1; nT_s)$ and $\hat{z}_2(f_0, T_{d2}, a_2; nT_s)$, do not overlap. The variance $\beta(nT_s \in L_3)$ increases when the echo models are fitted with the echo from the tissue below the adventitia layer that is false detection. Therefore, the estimation of $\beta(nT_s \in L_3)$ could prevent the echo below the adventitia layer from being detected. Overall, the misdetection of the LIB and MAB can be reduced by calculating such variances. Thereafter, the positions of the LIB and MAB echo models, $\hat{z}_1(f_0, T_{d1}, a_1; nT_s)$ and $\hat{z}_2(f_0, T_{d2}, a_2; nT_s)$, which give the minimum difference $\min\{\alpha(f_0, T_{d1}, T_{d2}, a_1, a_2; \tau_1, \tau_2)\}$ between the measured *in vivo* RF echo $x(nT_s)$ and echo model $\hat{z}(f_0, T_{d1}, T_{d2}, a_1, a_2; nT_s)$ are determined as the optimum positions of the LIB and MAB.

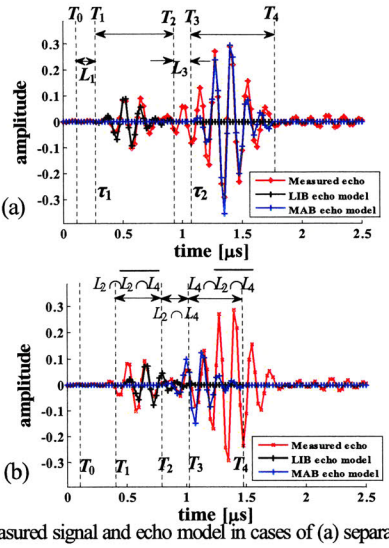

Figure 3 Measured signal and echo model in cases of (a) separated and (b) overlapped $\hat{z}_1(f_0, T_{d1}, a_1; nT_s)$ and $\hat{z}_2(f_0, T_{d2}, a_2; nT_s)$.

3. Accuracy Evaluation by Phantom Experiment

To evaluate the accuracy of the proposed method, a phantom experiment using a rubber sheet which mimics the carotid arterial wall and using a rubber sheet with a silicone board which mimics the carotid arterial wall and scatterrers below the adventitia layer were conducted. In the experiment, the modified ultrasonic diagnostic equipment (SSD-6500, ALOKA) was used. The scanning of the rubber sheet in water is performed using a 10-MHz linear array transducer (UST-5410, ALOKA), and the RF signals were sampled at 40 MHz at a 16-bit resolution. The acoustic focus was set at 20 mm and the electronic focus was set at 13.7 mm, associated with the distance between the transducer and the rubber sheet. The thickness of the rubber sheet was separately measured by a digital micrometer (MCD 191-30WD) for 10 times at difference position and the estimated average thickness was 449 μm. For mimicking scatterrers below the adventitia layer, silicone contained 2% of graphite and was covered by the rubber sheet. The sound velocity c_0 of the rubber sheet is estimated at 1561 m/s. In this research, the proposed method was validated to be better than the previous method.[6,7] The results of estimated rubber sheet thickness obtained from the proposed and previous methods for the experiments using a rubber sheet and using a rubber sheet with silicone board are concluded as shown in Table 1. It could be summarized that for both of the experiments in the 4 measurements, the results obtained from the proposed method have small percentage of differences from the true value, thus, the proposed method was verified to be more accurate than the previous method in detecting the boundaries. Figures 4(a) and 4(b) show the B-mode images with the detected boundaries obtained from the proposed method for the experiments using a rubber sheet and a rubber sheet with silicone board, respectively.

Table 1 Estimated rubber sheet thickness obtained by proposed and previous methods for the experiment using a rubber sheet and a rubber sheet with silicone board.

Measurement times	Experiment using a rubber sheet		Experiment using a rubber sheet with silicone	
	Proposed Method	Previous Method	Previous Method	Previous Method
	Average measured thickness±std (diff. between measured and true thicknesses)			
1	473.0±8.5 μm (5.3%)	529.6±93.0 μm (17.8%)	497.2±69.7 μm (10.7%)	635.0±81.1 μm (41.4%)
2	468.1±10 μm (4.2%)	493.3±66.4 μm (9.9%)	462.8±40.5 μm (3.1%)	624.0±90.4 μm (38.9%)
3	468.6±9.2 μm (4.3%)	545.3±103 μm (21.4%)	485.5±80.3 μm (13.1%)	599.3±103.3 μm (33.4%)
4	472.2±8.1 μm (5.1%)	522.7±95 μm (16.4%)	475.8±77.1 μm (5.9%)	625.3±75 μm (39.2%)

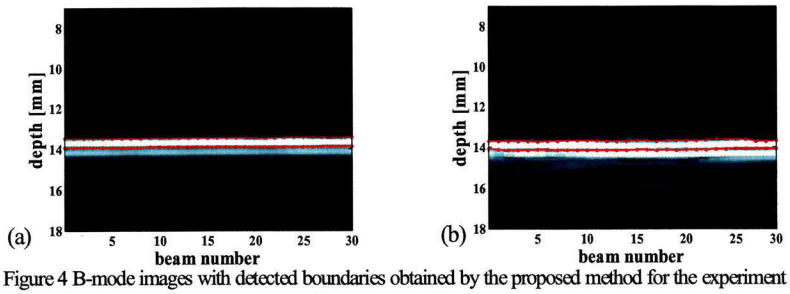

Figure 4 B-mode images with detected boundaries obtained by the proposed method for the experiment using (a) a rubber sheet and (b) a rubber sheet with silicone board below the sheet.

4. Boundary Detection in *In Vivo* Measurement

In the *in vivo* measurement, the same modified ultrasonic diagnostic equipment (SSD-6500, ALOKA) and 10-MHz linear array transducer (UST-5410, ALOKA) were used. The right carotid artery of healthy males at the ages of 23 and 36 were scanned and the RF signals were sampled at 40 MHz at a 16-bit resolution. By applying the MSE method as shown in eq. (4), two restrictions were set in this detection procedure. First, the amplitude of detected MAB echo should be larger than the amplitude of detected LIB echo. Second, since the average IMT is ranged from 0.39 mm to 0.62 mm for a healthy male of age between 17 and 63[9] and the IMT varies from person to person, in this work, the range of $0.5c_0(\tau_2-\tau_1)$ was scaled from 0.35 mm to 1 mm (c_0: sound velocity in tissue). Figure 5 shows the B-mode images of posterior carotid arterial walls with detected boundaries.

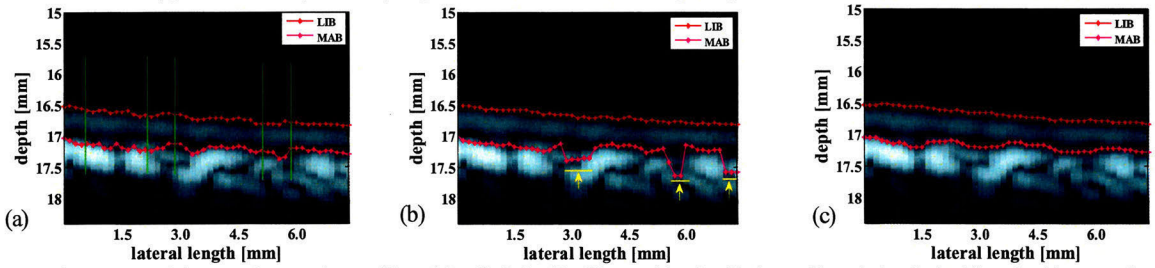

Figure 5 B-mode images of posterior carotid arterial wall of a healthy 23-year old male with detected boundaries obtained from the (a) proposed, (b) previous and (c) manual methods.

From these results, at some beam positions (marked by arrows with yellow lines in Fig. 5(b)), the boundaries estimated by the improved technique differ from those by the previous one. For all analyzed beams, only [4.8% - 27.5%] of $\min\{\alpha(f_0,T_{d1},T_{d2},a_1,a_2;\tau_1,\tau_2)\}$ convinces that the echo model used in this study is very good agreement with the measured *in vivo* RF echo. However, there are still small distortions appeared (around the beam indicated by green line in Fig. 5(a)) which desired to be improved. In the future work, to improve the detection of MAB by considering the multiple interfaces produced in the adventitia layer, multiple echo models should be employed to fit with the echo from the MAB instead of an echo model. As shown in Table 2, for the three healthy subjects, the average IMTs obtained from the proposed method showing the decrease of the standard deviations from those obtained from the previous method. Thus, the boundaries were detected with good reproducibility using the method proposed in this research which yields the better results than the previous method.

Table 2 Average IMTs obtained from the proposed, previous and manual methods and the differences between the one obtained from the proposed and that from the manual methods.

	IMTs obtained from the proposed method	IMTs obtained from the previous method	IMTs obtained from the manual method	Differences between the IMTs obtained from proposed and manual method	Differences between the IMTs obtained from proposed and manual method
Subject 1	502±61 μm	558±120 μm	504±65 μm	0.40%	10.70%
Subject 2	507±96 μm	550±120 μm	444±55 μm	14.10%	23.80%
Subject 3	468±57 μm	512±69 μm	435±45 μm	7.60%	17.70%

5. Conclusion

In this study, using the proposed template matching technique, the boundary positions of IMT in the posterior wall of the carotid artery are estimated realizing the better MAB detection. Moreover, for the accurate detection of the LIB and MAB, the frequency and initial phase of the echo model were considered to fit with the measured echo. In a nutshell, the results obtained from the improved proposed method showed advantage for the automatic detection of the IMT of the carotid arterial wall, and it would be useful for the diagnosis of early-stage atherosclerosis.

Reference

1. S. Mendis, P. Puska, and B. Norrving, (World Health Organization, Geneva, 2011) p. 3.
2. P. Pignoli, E. Tremoli, A. Poli, P. Oreste, and R. Paoletti, Circulation 74 (1986) 1399.
3. V. Savithri and S. Purushothaman, Int. J. Adv. Comp. Sci. App. 1 (2010) 78.
4. S. Golemati, J. Stoitsis, E. G. Sifakis, T. Balkizas, and K. S. Nikita, Ultrasound Med. Biol. 33 (2007) 1918.
5. Q. Liang, I. Wendelhag, J. Wikstrand, and T. Gustavsson, IEEE Trans. Med. Imag. 19 (2002) 127.
6. T. Kaneko, H. Hasegawa, and H. Kanai, Jpn. J. Appl. Phys. 46 (2007) 4881.
7. K. Ikeshita, H. Hasegawa, and H. Kanai, Jpn. J. Appl. Phys. 50 (2011) 07HF08-1.
8. N. Ibrahim, H. Hasegawa, and H. Kanai, Jpn. J. Appl. Phys. 51 (2012) 07GF07-1.
9. J. Gariepy, J. Salomon, N. Denarie, F. Laskri, J. L. Megnien, J. Levenson, and A. Simon, Arterioscler. Thromb. Vasc. Biol. 18 (1998) 584.

論文審査結果の要旨

動脈硬化症の診断において，動脈壁の断層像を非侵襲的に観察できる超音波診断装置が広く用いられている．動脈壁は内膜，中膜，外膜の3層構造を有するが，動脈硬化症ではその進行過程において，内膜に遊走した中膜平滑筋細胞の増殖などにより内膜が肥厚するため，動脈壁の厚みが動脈硬化の進行度を測る指標となる．超音波診断装置により得られる断層画像では，内腔-内膜境界および中膜-外膜境界からの反射超音波(エコー)が描出され，それらの境界検出により内膜中膜複合体の厚み(Intima-Media Thickness: IMT，健常者では0.5-1.0 mm程度)を計測できるため，非侵襲的な動脈硬化症の診断法として臨床において広く計測されている．特に頸動脈におけるIMT計測は簡便で，かつ頸動脈の動脈硬化進行度は冠動脈など他の動脈における進行度とも相関することから，頸動脈における計測が一般的である．IMT計測において，超音波断層画像を解析してIMTを自動計測する手法も開発されているが，精度の点から依然手動で計測を行うのが主流である．本論文は，受信した動脈壁からの反射超音波信号の解析によるIMTの自動計測に関する研究をまとめたものであり，全編5章からなる．

第1章は序論であり，本研究の背景，目的及び構成を述べている．

第2章では，提案する受信超音波信号の解析法を述べている．既に実用化されているIMT自動計測法は超音波画像の解析に基づくため，受信信号の振幅情報しか利用していない．それに対し本研究グループでは，振幅に加え位相情報も含む超音波RF (Radio-Frequency)信号を利用して高精度なIMT計測を実現しており，これまでに手動計測に比較し誤差10%程度の精度を達成している．本研究では，さらに詳細な信号解析法を開発し，更なる精度向上を図っている．そのため点散乱体からの受信超音波パルス信号を超音波ハイドロホンで計測し，テンプレート波形として予め用意する．次に血管からの受信信号をテンプレートとマッチングさせることで，反射源をパルス状信号として検出する．さらに，超音波はその伝播過程で伝播遅延，周波数依存減衰による中心周波数の低下が生じるため，整合を行う際にテンプレート波形の初期位相と周波数を変化させ，整合度の向上を図っている．その結果，従来は25.3%であった整合誤差を8.3%まで低減できることを示している．これは優れた成果である．

第3章では，動脈壁を模擬したゴム板を用いて，精度評価実験を行っている．0.45 mmの厚さのゴム板について計測を行い，計測誤差を従来法の16.4%から本手法で5.1%まで，標準偏差を18.1%から1.7%まで低減できることを示した．この結果は，本研究で開発した信号解析手法の有効性を示す重要な成果である．

第4章では，ヒト頸動脈を計測して得られた受信超音波信号に，第2章の手法を適用している．手動により計測したIMTに対する誤差を評価し，従来法の誤差13.0%に対し，提案手法を用いることで3.0%まで大幅に誤差を低減可能であることを示している．これは臨床計測における有用性を示す優れた成果である．

第5章は結論である．

以上要するに本論文は，振幅・位相両方の情報を含む超音波RF信号を解析することによりIMTを高精度に自動計測する手法について述べたものであり，基礎実験による精度評価および頸動脈のin vivo計測から本手法の有効性や臨床応用の可能性を示しており，電子工学および医用超音波工学の発展に寄与するところが少なくない．

よって，本論文は博士(工学)の学位論文として合格と認める．